One-dimensional confinement effect in hematite quantum rod arrays

Lionel Vayssieres
International Center for Young Scientists, National Institute for Materials Science, Tsukuba, Japan 3050044

ABSTRACT

Synchrotron-based spectroscopic investigations of 1-D nanomaterials consisting of designed oriented nanorod-arrays of hematite grown by aqueous chemical growth reveal significant differences in the electronic structure and bandgap compared to bulk samples. Resonant inelastic x-ray scattering (RIXS) study of α-Fe_2O_3 crystalline nanorod bundle arrays at the Fe *L*-edge is reported. The low energy excitations, namely *d-d* and charge-transfer excitations, are identified in the region from 1 to 5 eV. The 1-eV and 1.6-eV energy-loss features are weak transitions from multiple excitations. The 2.5-eV excitation which corresponds to the bandgap transition appears significantly larger than the typical 1.9-2.2-eV-bandgap of single-crystal or polycrystalline hematite samples, revealing a one-dimensional (1-D) quantum confinement effect in the bundled ultrafine nanorod-arrays. Such conclusion strongly suggest that bandgap and band edge position criteria for direct photo-oxidation of water by solar irradiation without an applied bias are therefore satisfied for such purpose-built nanomaterials. The outcome of such a result is of great importance for the solar production of hydrogen, an environmental friendly energy source carrier for the future. Indeed, the generation of hydrogen by visible light irradiation with an environmental friendly and economical photoactive material would thus advance a step closer to reality.

Keywords: metal oxide, nanostructure, quantum confinement, nanorod, one-dimensional, semiconductor, electronic structure, synchrotron radiation, iron oxide

1 INTRODUCTION

Iron compounds are essential materials in chemistry, biology and geology due to their large occurrence in nature[1], for instance, in water[2], plants[3], minerals[4] and clay minerals[5], sediments[6], and sedimentary rocks[7]. The molten core of the Earth is primarily elemental iron, which is the fourth most abundant element in the Earth's crust and is found in significant amount in Martian soil[8]. The oxides of iron play a central role in geochemistry of soil[9], in planetary science[10], and contribute for instance, to the oxidation of sedimentary organic matter[11]. In its various allotropic forms, iron oxides and oxyhydroxides represent important basic and raw materials[12]. Their large abundance, non-toxicity, low-cost, high refractivity, and various colors, contribute to their popularity as polishing agents, and for colorants (red and yellow ochre) for the pigment and paint industry. Indeed, iron oxides are the most commonly used colored pigments in the paints and coatings market[13]. It is also widely studied for the alloys and steel industry[14], in metallurgy[15], as catalysts[16-18] and photocatalysts[19], for magnetic storage devices, cathodes for primary and secondary batteries[20], chemical flame suppressant[21] and for the crucial industrial, economical and environmental issue of corrosion[22]. The thermodynamically stable crystallographic phase of ferric oxides is hematite (α-Fe_2O_3) which represents the most important ore of iron considering its high iron content and its natural abundance. Therefore, designing iron(III) oxides with a novel, anisotropic and highly oriented morphology is of great fundamental importance for basic physical, earth and life sciences and of relevance for various fields of industrial applications.

Bandgap, band edge positions as well as the overall band structure of semiconductors are of crucial importance in photoelectrochemical and photocatalytic applications. The energy position of the band edge level can be controlled by the electronegativity of the dopants, solution pH (flatband potential variation of 60 mV per pH unit), as well as by quantum confinement effects. Accordingly, band edges and bandgap can be tailored to achieve specific electronic, optical or photocatalytic properties. A very important application is found in the generation of H_2 from direct photo-oxidation of water without external bias[23]. Indeed, to succeed in splitting water via solar irradiation, the valence band of the semiconductor has to be located at a lower energy level than the chemical potential of dioxygen evolution (H_2O/O_2), and the conduction band has to be located at a higher energy level than the chemical potential of dihydrogen evolution (H_2/H^+). If the position of the energy levels of the valence and conduction band is not fulfilled, an external bias has to be applied to induce the photocatalytic process, which in turn substantially reduces the overall efficiency. It has been reported that the optimal band gap of 2.46 eV[24] is required for water photo-oxidation without an external bias. Although

Solar Hydrogen and Nanotechnology, edited by Lionel Vayssieres
Proc. of SPIE Vol. 6340, 63400O, (2006) · 0277-786X/06/$15 · doi: 10.1117/12.678301

the bandgap of hematite, reported to be around 1.9 to 2.2 eV (depending on its crystalline status and methods of preparation), and its valence band edge are suitable for oxygen evolution, the conduction band edge of hematite is too low to generate hydrogen. Therefore, a blue shift of the bandgap of hematite of about 0.3 to 0.6 eV and the concomitant upward shift of the conduction band edge would make hematite an ideal anode material for photocatalytic devices for the photo-oxidation of water in terms of cost, abundance, non-toxicity, as well as thermal and structural stability and photo-corrosion resistance. Efficient photovoltaic properties have been demonstrated by the design of thin films of hematite consisting of crystalline arrays of oriented nanorods[25]. They exhibited substantial photocurrent efficiency due to a better transport and collection of photogenerated electrons through a designed path (i.e. the oriented rods) as well as better physical and structural match between the n-type semiconductor material, the diameter of its nano building blocks and the minority carrier (hole) diffusion length[26]. In the present report, we investigate quantum confinement effects on bandgap profiling in similar arrays by resonant inelastic x-ray scattering (RIXS) of synchrotron radiation for potential application of such nanomaterials in direct photo-oxidation of water by solar irradiation.

2 METHODOLOGY

Such an approach has been successfully applied to develop a new generation of functional materials, the so-called *purpose-built materials*[27]. Indeed, when the thermodynamic stabilization concept[28] is applied to heterogeneous nucleation rather than homogeneous nucleation, not only the size of spherical nanoparticles can be controlled[29] but also the shape and the orientation of anisotropic building blocks onto various substrates can be tailored to build smart and functional nanostructures[30]. Thus, the fabrication of highly oriented crystalline arrays[31] of large physical area consisting of nanorods of iron oxides[25], iron-chromium sesquioxide nanocomposites[32], iron oxyhydroxides and iron metal[33] have been successfully designed by following such ideas. In addition, ZnO nanorods and nanowires[34], microrods[35], microtubes[36] along with other morphologies[37], nanowires and nanoparticles of manganese oxides[38] and arrays consisting of sub-monolayers of non-aggregated mesoparticles of α-Cr_2O_3[39] have also been obtained by such strategy. Figure 1 illustrates some of the achievements in advanced iron oxide nanomaterials (thin films and arrays) design from aqueous solutions at low temperature. More recently, ordered arrays of *c*-axis elongated nanorods of rutile SnO_2[40] (cassiterite) with square cross-section have also been successfully fabricated following the same concept and aqueous thin film processing method. Such purpose-built nanomaterials have been designed for instance to improve the photovoltaic and photoelectrochemical[41] and gas sensing[42] properties of large band gap semiconductors[43]. Better fundamental understandings of the electronic structure[44] and orbital symmetry contribution of II-VI semiconductor nanomaterials[45] as well as quantum confinement effects in TiO_2 quantum dots as well as SnO_2 and α-Fe_2O_3 ultrafine nanorods[46] have also been obtained with such materials. Finally, the direct application of such model allowed the demonstration of the thermodynamic stabilization of metastable crystal phases such as hydroxides and oxyhydroxides of transition metals in aqueous solutions[47] as well as the fabrication of novel bio-nanocomposites by tailoring the conformation of bioactive molecules adsorbed on metal oxide nano-arrays[48]

RIXS experiments were conducted on beamline 7.0.1[49] at the Advanced Light Source, Lawrence Berkeley National Laboratory. The photon energy resolution was set to 0.2 eV for x-ray absorption spectroscopy (XAS) measurements at Fe L-edge. RIXS spectra were recorded using a grazing-incidence grating spectrometer[50]. The resolution of the monochromator and the fluorescence spectrometer were both set to 0.5 eV. X-ray absorption and emission spectra were collected at room temperature with a base pressure below 5.10^{-9} torr. The intensity of the signal is normalized to the beam current to account for the decay of the synchrotron radiation during the measurements.

The measurements were performed on hematite nanorods grown directly onto substrates by controlled aqueous chemical growth[30]. The investigated samples are thin films which consist of three dimensional crystalline arrays of hematite nanorod bundles of 50 nm in diameter and 500 nm in length (aspect ratio 1:10) perpendicularly oriented onto the substrate. Each bundle was found to consist of quantum rods of typically 4-5 nm in diameter (aspect ratio 1:100) as seen in figure 1. The thin films samples were prepared by direct (heteronucleation) growth and thermodynamic stabilization of β-FeOOH onto various substrates (e.g. transparent conductive oxides and sapphire) by the hydrolysis-condensation of an aqueous solution consisting of 0.1M of $FeCl_3$ and 1M $NaNO_3$ at pH 1.25 at 95°C for 10 hours. The *yellow* β-FeOOH thin films consisting of oriented nanorods are thoroughly rinsed with water and subsequently heated in air at 550°C for one hour to allow a complete crystal phase transition with conservation of the anisotropic morphology to the *orange-red* hematite (α-Fe_2O_3) as confirmed by thin film x-ray and electron diffraction as well as by thermal analysis.

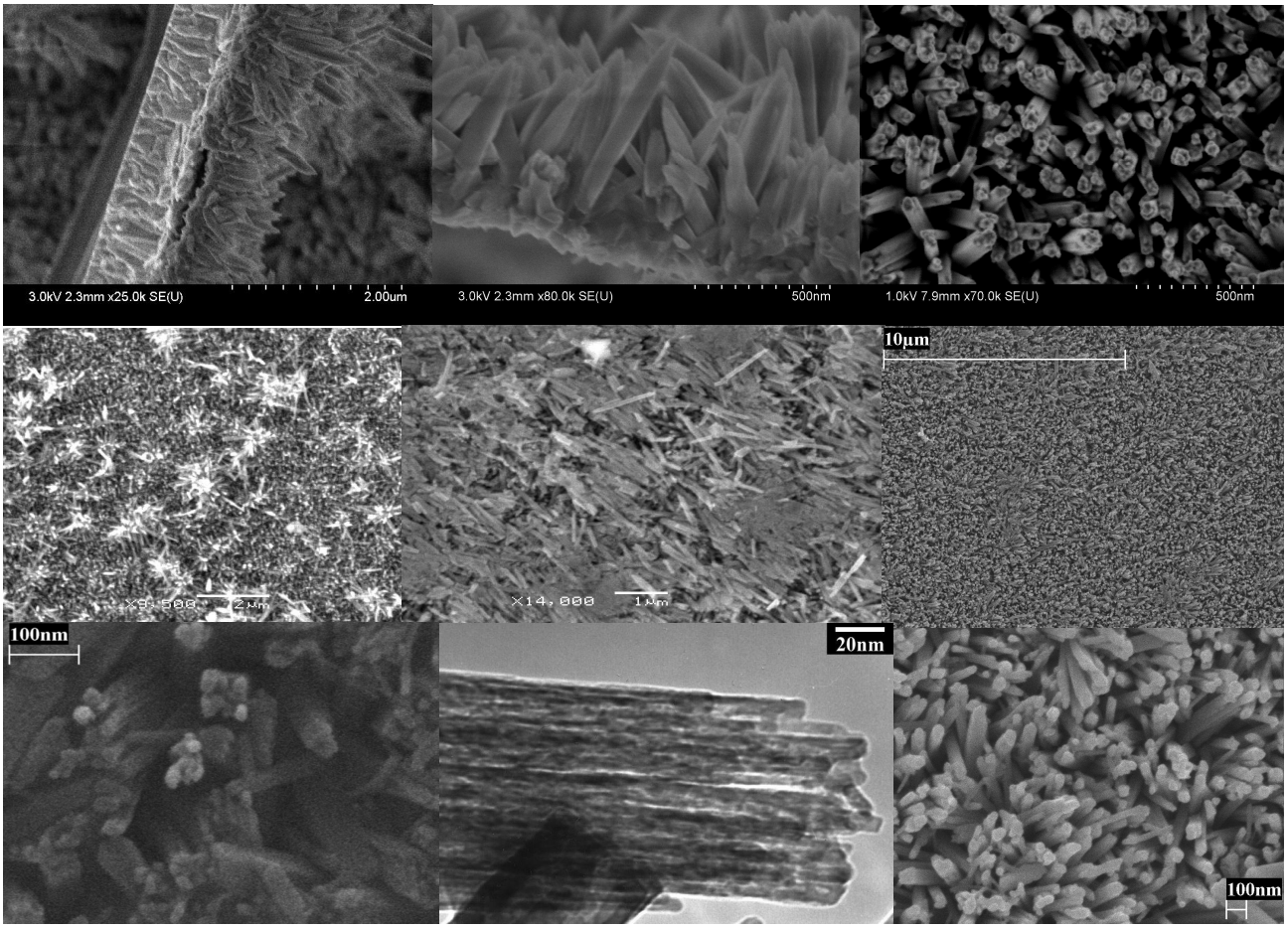

Figure 1: Electron micrographs of various α-Fe_2O_3 oriented nanorod-arrays and quantum rod bundle.

3 STRUCTURAL DESCRIPTIONS

The formation of such bundles of hematite nanorods is understood by considering the crystal structure of β-FeOOH which occurs in nature as the mineral akaganeite. It crystallizes in the tetragonal system (space group I4/m, a = 10.44, c = 3.01 Å). Its structure can be described as a tunnel structure (similar to α-MnO_2) hosting H_2O or Cl^- and is based on a defected close packed oxygen lattice with three different kinds of oxygen layers (figure 2, left). Every third layer is only two-third occupied with rows of oxygen atoms missing along the *c*-axis. The cation occupation of octahedral sites between the other anion layers is in double rows, but separated by single rows of empty sites along *c*. The octahedral cation sites remaining between the third anion layer and its neighbor layer are completely filled. This topology produces di-octahedral chains, which are arranged around the four-fold symmetry *c*-axis. The chains share vertices along their edges, forming square-cross section tunnels, some 0.5 nm on edge. Although such tunnels appear wide, only a single row of oxygen is missing. The crystal habit is rod shaped grouping of 5x5xn unit cells where n refers to replication along the c-axis. These crystals have empty cores, that is, a 3x3xn cell hole runs down the center of the crystal, producing a square channel of about 3 nm on a side. The anisotropic nanocrystals form bundles called somatoids. The dehydration of β-FeOOH nanorods at high temperature leads to the thermodynamically stable phase of Fe(III) oxide, the α-Fe_2O_3 phase, that has an anisotropic morphology consisting of bundled nanorods. The empty cores (channels) of the β-FeOOH structure become filled in the α-Fe_2O_3 structure resulting from the difference in packing density of the two structures.

The dehydration of β-FeOOH at high temperature (above 400°C) leads to the thermodynamically stable α-Fe_2O_3 phase. Thermal analysis of β-FeOOH nanorods shows a low overall weight loss of 3.75% within the range of 100-600° C. A 0.5% loss due weakly bonded water molecules occurs until 200°C. Most of the weight loss (3%) is occurring between

200 and 300°C accompanied by a broad endothermic shoulder which corresponds to the evaporation of structural water. A very sharp exothermic peak occurs at 385°C with a concomitant 0.2% loss of water corresponding to the crystal phase transition to hematite. A continuous slow decay of the TGA curve is observed until 600°C corresponding to the slow process of diffusion and evaporation of surface/bulk OH groups as H_2O with a very small exothermic peak at 540°C[51].

Hematite crystallizes in the trigonal crystal system, space group R-3c, and is isostructural with corundum (α-Al_2O_3). The unit cell can be described as rhombohedral with three equal axes a = 5.43 Å and an angle between edges α = 55°18' containing two formula unit (Z=2), or hexagonal with a = 5.03 Å and c = 13.75 Å (Z=6). The lattice is built on a hexagonal close packed (HCP) array of oxygen with four of every six available octahedral sites around O atoms occupied with Fe (figure 2, right). The octahedral and tetrahedral sites are above and below one another in a HCP lattice, the tetrahedral sites remaining empty. Octahedra are sharing faces along a threefold axis and are distorted to trigonal antiprisms because of the Fe-Fe repulsion occurring across one shared face and not the others. This yields to a very dense structure (i.e. high oxygen packing index), showing a high polarisability and a high refractive index.

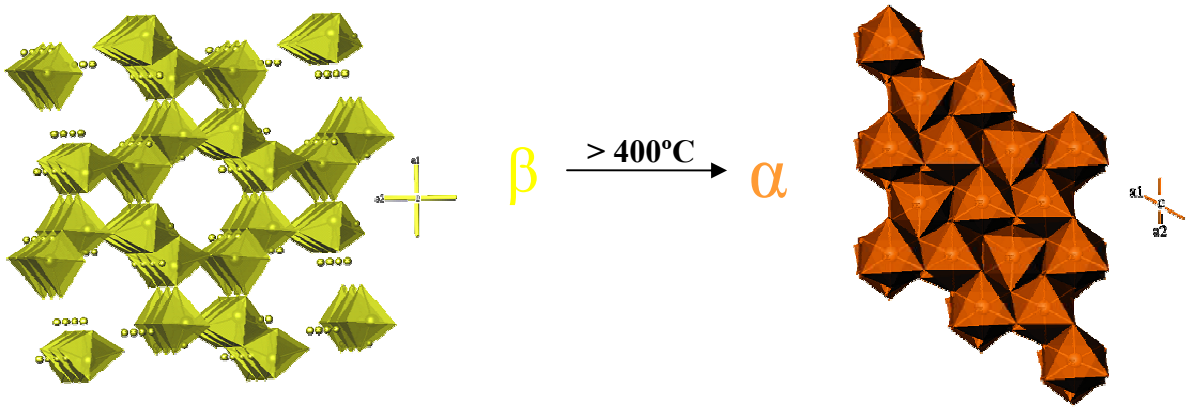

Figure 2: Crystal structure representations (projected along the c-axis) of β-FeOOH, akaganeite (left) and α-Fe_2O_3, hematite (right).The crystal phase transition between akaganeite and hematite occurs above 400°C

3 RESULTS

Figure 3 shows the x-ray absorption spectra (XAS) of hematite nanorod-array at O K-edge. The oxygen K-edge spectrum (1s → 2p) shows two regions corresponding to oxygen 2p orbitals hybridized respectively, with Fe 3d orbitals (530-535 eV) and with Fe 4s,4p orbitals (535-550 eV).

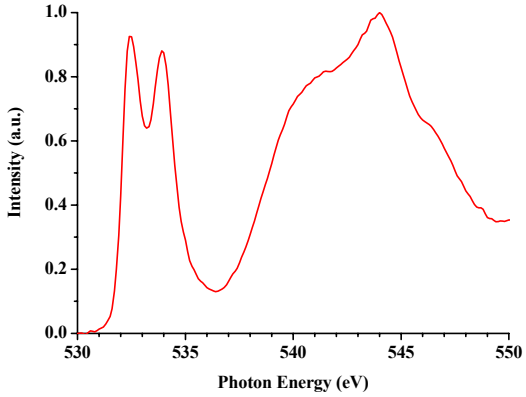

Figure 3: X-ray absorption spectra at O K-edge of α-Fe_2O_3 nanorod-array.

The Fe 2*p* absorption spectrum of the α-Fe_2O_3 nanorod array is displayed in figure 4a. The spectral shape appears very similar to previous XAS measurements conducted on polycrystalline[52] or single-crystal[53] samples. The typical

spectrum shows the spin-orbit interaction of the 2*p* core level that splits the L_2 ($2p_{1/2}$) and L_3 ($2p_{3/2}$) edges, and the *p-d* and *d-d* Coulomb and exchange interactions that cause multiplets within the edges. The ligand field splitting of *3d* transition metals, being of the same order of magnitude as *p-d* and *d-d* interactions (1-2 eV), gives a 1.4-eV-energy splitting between the t_{2g} (*xy, yz , xz*) and e_g (x^2-y^2, $3z^2$-r^2) orbitals. The charge transfer has two main effects on the spectral shape[54]. It splits *d* levels by the formation of molecular orbitals as well as giving rise to an asymmetric shape (tail). Such effects can clearly be observed on the higher-energy side of the edges, especially in the 711-718 eV regions (L_3) of the experimental spectrum (figure 4a).

Figure 4b shows the Fe *L*-emission spectrum recorded with a higher photon-energy excitation (*ca* 750 eV). The spectral shape shows two peaks originating from the transitions of *3d* orbitals to $2p_{1/2}$ and $2p_{3/2}$ core levels. A branching ratio (L_β/L_α) of 0.8 is found for the α-Fe_2O_3 bundled nanorod arrays, which appears substantially larger than that of α-Fe_2O_3 single crystal[53] (figure 4d). It has been demonstrated that the intensity ratio $I(L_\beta)/I(L_\alpha)$ varies due to the occupancy of L_2 and L_3 levels, which depends on the chemical state of the elements[55]. Skinner *et al.*[56] showed that the ratio $I(L_\beta)/I(L_\alpha)$ of *3d* transition metals and alloys is very small due to the non-radiative Coster-Kronig transition $L_2L_3M_{4,5}$. The probability of such a transition is distinctly lower for 3*d* oxides than for metals due to the presence of an energy gap. Recently, Kurmaev[57] *et al.* found that the ratio $I(L_\beta)/I(L_\alpha)$ of the molecular superconductor $(ET)_4[(H_3OFe(C_2O_4)_3]C_6H_5CN$ was twice as great as that of iron oxides because of the highly ionic and insulating character of the oxalate layers as well as the localization of the 3*d* electron density. The present experimental observation of a higher branching ratio $I(L_\beta)/I(L_\alpha)$ suggests the possibility of a larger bandgap in hematite nanorod. Resonant inelastic x-ray scattering at core resonances has become a new tool for probing the optical transitions in transition metal oxides[58]. A scheme of the RIXS process is presented in the inset of Figure 5. In the case of hard x-ray K-edge RIXS process, the intermediate state in a transition metal is the same as the final state in a K-edge absorption measurement, while the RIXS final state (when scanning the K-edge region) are the same as in L-edge absorption spectroscopy. For L-edge and M-edge RIXS, the final states are typically d-d or f-f excitations[59]. The formulations of RIXS lead to a Kramers-Heisenberg type dispersion formula for the cross section with generally only the resonant part of the scattering process taken into account. Second-order perturbation theory for the RIXS process leads to the Kramers-Heisenberg formula for the resonant x-ray scattering amplitude. The lowest-lying electronic excitations can be studied most directly by charge neutral spectroscopies, such as electron energy-loss spectroscopy (EELS) and optical absorption. The *d-d* excitations in transition metal compounds are dipole forbidden and are therefore very faint in optical spectroscopy. In the RIXS process, final states probed via such a channel are related to eigenvalues of the ground state Hamiltonian. The core-hole lifetime does not limit the resolution of this spectroscopy. According to the many-body picture, the energy of a photon, scattered on a certain low-energy excitation, should change by the same amount as a change in an excitation energy of the incident beam (see the decay route of core-excitations e_g versus that of t_{2g} in the inset of figure 5), so that RIXS features have constant energy losses and follow the elastic peak on the emitted-photon energy scale. In such an octahedral symmetry, a d^5-configuration is found to have well-separated *d-d* excitations. Optical absorption spectroscopy of α-Fe_2O_3 has revealed many transitions ranging from infrared to ultraviolet region. In a typical spectrum, well-defined features are observed at 2.1 eV, 3.3 eV, and 5.6 eV[60], which are assigned to the following electronic transitions ${}^6A_1 \rightarrow {}^4A_1, {}^6t_{1u} \rightarrow {}^2t_{2g}$, and ${}^6t_{1u} \rightarrow e_g$, respectively. These features are also found in the RIXS spectrum of a α-Fe_2O_3 single crystal[53]. In such a process, the *d-d* excitations in α-Fe_2O_3 are specifically probed by the transition sequence $2p^63d^5 \rightarrow 2p^53d^6 \rightarrow 2p^63d^5$. These *d-d* transitions become fully allowed, and their intensity can be more easily calculated compared to optical spectroscopy and EELS. The RIXS spectrum recorded at the Fe *L*-edge of α-Fe_2O_3 nanorods is shown in figure 5. Several energy-loss features are clearly resolved. The low energy excitations, such as the strong *d-d* and charge-transfer excitations, are identified in the region from 1 to 5 eV. The 1-eV energy-loss features originate from multiple excitation transitions. The 4.1 and 6.4 eV excitation originates from charge transfer between oxygen 2*p* and iron 3*d* orbitals. The 2.5-eV excitation, which corresponds to the bandgap transition of hematite, appears significantly blue shifted compared to the reported 1.9~2.2 eV bandgap of single-crystal and polycrystalline samples as suggested above by the higher L_β/L_α branching ratio observed in the *L*-emission spectrum of the nanorods (figure 4b) compared to the single crystal (figure 4d). Such direct observation of a substantial (0.3-0.6 eV) bandgap increase is successfully attributed to a 1-D (lateral dimension) quantum confinement effect in the designed bundled ultrafine nanorods of hematite. Such findings strongly suggest that such designed nanomaterials would meet the bandgap[24] requirement for the photocatalytic oxidation of water without an applied bias. In addition, one may argue with confidence that such nanomaterials will also meet the conduction band edge requirement for generation of hydrogen without applied bias (figure 6). Indeed, if the valence band edge is pinned, the increase in bandgap should be sufficient to reach the chemical potential of dihydrogen evolution. If both valence band edge and conduction band edge

are concomitantly moving upward, the increase in bandgap would certainly be sufficient to locate the conduction band edge of hematite above the chemical potential of (H_2/H^+) allowing the generation of hydrogen from iron oxide materials by visible (solar) illumination without applied bias.

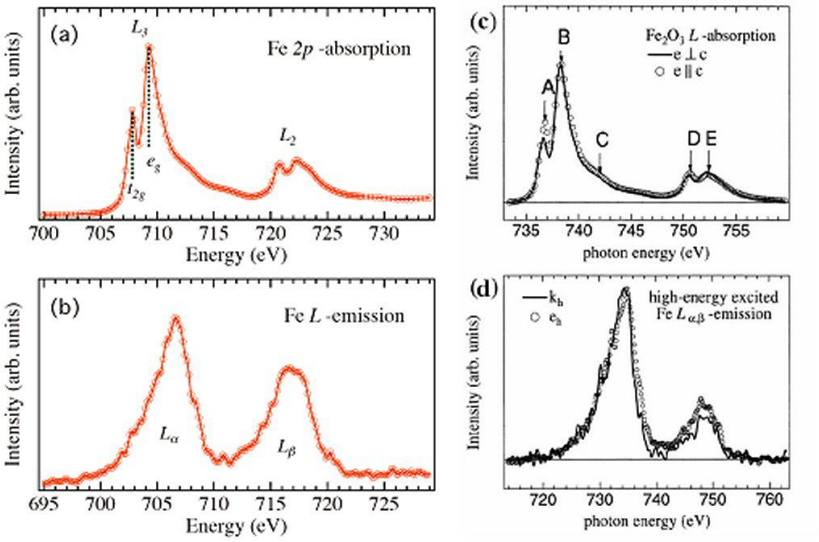

Figure 4: Fe 2p absorption (top) and normal L-emission (bottom) spectra of α-Fe_2O_3 quantum rod-array (a, b) and of single crystal sample (c, d) from reference 54

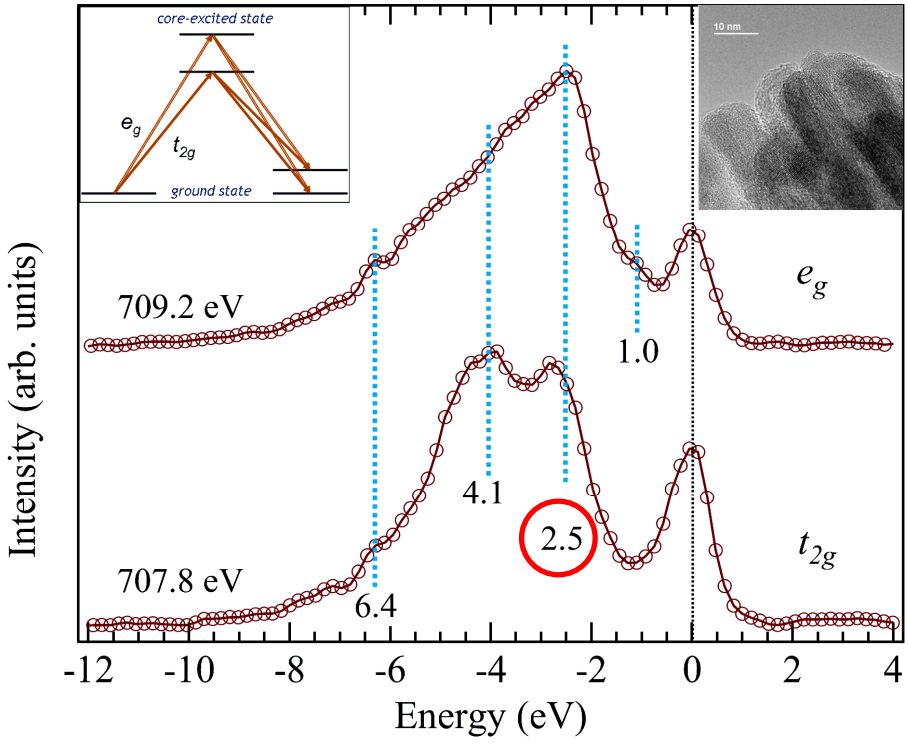

Figure 5: Energy dependent resonant inelastic x-ray scattering (RIXS) spectra of α-Fe_2O_3 quantum rod arrays. The left inset shows the schematic representation of the radiative de-excitation for the two core excitations e_g and t_{2g} involved in the RIXS process. The right inset shows a high resolution transmission electron microscopy image of the hematite rods.

Originally, such *purpose-built* perpendicularly oriented nanorod-arrays of hematite have been used to develop photovoltaic cells. Indeed, the diameter of the nanorods allows a perfect match with the minority carrier diffusion length of hematite. Accordingly, a very efficient photogenerated charge separation was obtained as well as a high incident photon to electron conversion efficiency of ca. 60% at 350 nm, which led to the creation of a 2-electrode hematite photovoltaic cells[26]. Besides the well-designed direct, grain boundary-free, electron pathway and the excellent structural match with the hole diffusion length, the presently investigated one-dimensional quantum confinement was suggested to account for the unusual high efficiency of the hematite nanorod-array photoanode. At present, novel devices based on quantum-confined oriented nanorod-arrays of hematite are under scrutiny at our laboratories for photocatalytic decomposition of water[61] without applied bias.

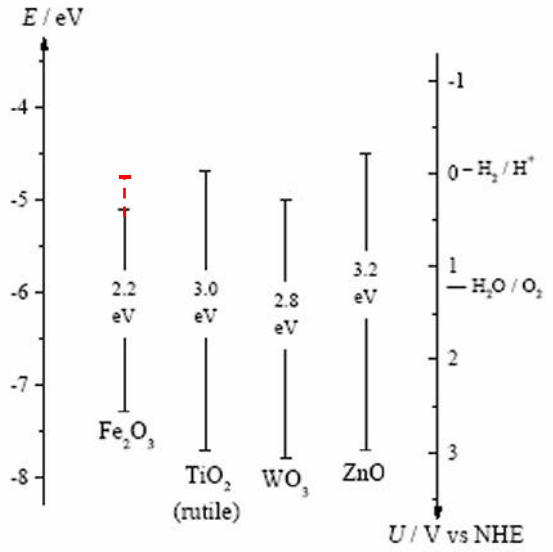

Figure 6: Survey of bandgap and band edge positions of major metal oxide semiconductors and chemical potentials of H_2/H^+ and H_2O/O_2. The dashed line represents the bandgap increase observed in the hematite nanorod arrays.

4 CONCLUSIONS

As a conclusion, the direct observation of a 1-D quantum confinement effect has been demonstrated in designed oriented bundles of ultrafine nanorods of hematite by resonant inelastic x-ray scattering. The bandgap (and most certainly the conduction band edge) criteria for direct photo-oxidation of water by solar irradiation without an applied would be satisfied for such purpose-built nanomaterials. The outcome of such a result is of great importance for a safe and economical solar production of hydrogen, an environmental friendly energy source carrier for the future.

.

ACKNOWLEDGEMENTS

This work was supported by special coordination funds for promoting Science and Technology from the Ministry of Education, Culture, Sports, Science and Technology of Japan. The work at the ALS and LBNL was supported by the Director, Office of Basic Energy Sciences, Division of Materials and Division of Chemical Sciences, Geosciences, and Biosciences of the U.S. Department of Energy at Lawrence Berkeley National Laboratory under contract No. DE-AC03-76SF00098.

REFERENCES

1. J. L. Jambor, J. E. Dutrizac, "Occurrence and constitution of natural and synthetic ferrihydrite, a widespread iron oxyhydroxide", *Chem. Rev.* 1998, *98*, 2549-2585
2. W. Stumn, J.J. Morgan, *Aquatic Chemistry* (Wiley, 1996)
3. G. Winklemann, F. Van der helm, J. B. Neidlans, *Iron transport in Microbes, Plants and Animals* (VCH, 1987).
4. L. A. J. Garvie, P. R. Buseck, "Ratios of ferrous to ferric iron from nanometre-sized areas in minerals", *Nature* 1998, *396*, 667-670
5. J. E. Kostka, E. Haefele, R. Viehweger, J.W. Stucki, "Respiration and dissolution of iron(III) containing clay minerals by bacteria", *Environ. Sci. Technol.* 1999, *33*, 3127-3133
6. H. M. Bao, P. L. Koch, R. P. Hepple, "Hematite and calcite coatings on fossil vertebrates", *J. Sediment. Res.* 1998, *68(5)*, 727-738
7. B. B. Ellwood, K. M. Petruso, F. B. Harrold, D. Schuldenrein, "High-Resolution paleoclimatic trends for the Holocene identified using magnetic susceptibility data from archaeological excavations in caves", *J. Archeological Sci.* 1997, *24*, 569-573
8. R.V. Morris, D.C. Golden, T.D. Shelter, H.V. Lauer, "Lepidocrocite to maghemite to hematite: A pathway to magnetic and hematitic Martian Soil", *Meteorit. Planet. Sci.* 1998, *33(4)*, 743-751
9. W. Stumm, B. Sulzberger, "The cycling of iron in natural environment", *Geochim. Cosmochim. Acta* 1992, *56(8)*, 3233-3257
10. G. Kletetschka, P. Wasilewski, P. Taylor, "Hematite vs. magnetite as the signature for planetary magnetic anomalies? ", *Phys. Earth Planet. In.* 2000, *119*, 259-267
11. D. R. Lovley, "Dissimilatory Fe(II) and Mn(IV) reduction", *Microbiol. Rev.* 1991, *55(2)*, 259-287.
12. R. M. Cornell, U. Schwertmann, *The Iron Oxides* (VCH, 1996)
13. P. G. Morse, "Paints & coatings", *Chem. Eng. News* 1998, *76(41)*, 42-62
14. K. Tano, E. Öberg, P. O. Samskog, T. Monredon , A. Broussaud, "Comparison of control strategies for a hematite processing plant", *Powder Technol.* 1999, *105*, 443-450
15. A. Von Ropenack, in J.E. Dutrizac , A.J. Monhemius Eds. *Iron control in Hydrometallurgy* (Ellis Horwood, 1986) pp. 730-741
16. R. Pestman, R.M. Koster, E. Boellaard, A.M. Van der Kraan, V. Ponec, "Identification of the active sites in the selective hydrogenation of acetic acid to acetaldehyde on iron oxide catalysts", *J. Catal.* 1998, *174*, 142-152
17. S-S. Lin, M. D. Gurol, "Catalytic decomposition of hydrogen peroxide on iron oxide: Kinetics, mechanism, and implications", *Environ. Sci. Technol.* 1998, *32*, 1417-1423
18. Y. Zhang, J. E. Ellison , J.C. Cannon, "Interaction of iron oxide with barium peroxide and hydroxide during the decomposition of sodium chlorate", *Ind. Eng. Chem. Res.* 1997, *36(5)*, 1948-1952
19. A. Duret, M. Grätzel, "Visible light-induced water oxidation on mesoscopic α-Fe_2O_3 films made by ultrasonic spray pyrolysis", *J. Phys. Chem. B* 2005 *109*(36) 17184-17191; E. L. Miller, D. Paluselli, B. Marsen, R. E. Rocheleau, "Development of reactively sputtered metal oxide films for hydrogen-producing hybrid multijunction photoelectrodes", *Sol. Energy Mater. Sol. Cells* 2005, 88(2), 131-144
20. S. Licht, B. Wang, S. Ghosh, "Energetic iron(VI) chemistry: The super-iron battery", *Science* 1999, 285, 139-1042
21. C. B. Kellog, K. K. Irikura, "Gas-phase thermochemistry of iron oxides and hydroxides: Portrait of a super-efficient flame suppressant", *J. Phys. Chem. A* 1999, *103(8)*, 1150-1159
22. S. E. Oh, D.C. Cook, H.E. Townsend, "Atmospheric corrosion of different steels in marine, rural and industrial environments", *Corrosion Sci.* 1999, *41*, 1687-1702
23. Z. Zhou, J. Ye, K. Sayama, H. Arakawa, "Direct splitting of water under visible light irradiation with an oxide semiconductor photocatalyst", *Nature* 2001, *414*, 625-627
24. Y. Matsumoto, "Energy positions of oxide semiconductors and photocatalysis with iron complex oxides", *J. Solid State Chem.* 1996, *126(2)*, 227-234
25. L.Vayssieres, N. Beermann, S.-E. Lindquist, A. Hagfeldt, "Controlled aqueous chemical growth of oriented three-dimensional nanorod Arrays: Application to Iron(III) oxides", *Chem. Mater.* 2001, *13(2),* 233-235
26. N. Beermann, L.Vayssieres, S.-E. Lindquist, A. Hagfeldt, "Photoelectrochemical studies of oriented nanorod thin films of Hematite", *J. Electrochem. Soc*. 2000, *147(7),* 2456-2461
27. L.Vayssieres, A. Hagfeldt, S.-E. Lindquist, "Purpose-Built Metal Oxide Nanomaterials. The emergence of a new generation of smart materials", *Pure Appl. Chem*. 2000, *72(1-2),* 47-52

28. L. Vayssieres, "On the thermodynamic stability of metal oxide nanoparticles in aqueous solutions", *Int. J. Nanotechnology* 2005*, 2(4),* 411-430 ; L. Vayssieres, "Précipitation en milieu aqueux de nanoparticules d'oxydes: Modélisation de l'interface et contrôle de la croissance", *PhD. Thesis,* Université Pierre et Marie Curie, Paris, France (1995), pp. 1-145
29. L.Vayssieres, C. Chaneac, E. Tronc, J.P. Jolivet, "Size tailoring of magnetite particles formed by aqueous precipitation: An example of thermodynamic stability of nanometric oxide particles", *J. Colloid Interface Sci*. 1998, *205(2),* 205-212
30. L.Vayssieres, "On the design of advanced metal oxide nanomaterials", *Int. J. Nanotechnology* 2004*, 1(1-2),* 1-41; L.Vayssieres, A. Hagfeldt, S.-E. Lindquist, "Purpose-Built Nanostructured Ru/RuO_2 thin films on plastic substrate for electrocatalysis applications", *The Electrochemical Society Meeting Abstracts* 1999, *99(2),* 2118
31. L.Vayssieres, "Purpose-Built Metal Oxide Nanomaterials. The emergence of a new generation of smart materials", *Pure Appl. Chem*. 2006, *78(9),* 1745-1751
32. L.Vayssieres, J.-H. Guo, J. Nordgren, "Aqueous chemical growth of αFe_2O_3-αCr_2O_3 nanocomposite thin films", *J. Nanosci*. *Nanotechnol.* 2001, *1(4),* 385-388
33. L.Vayssieres, L. Rabenberg, A. Manthiram, "Aqueous chemical route to ferromagnetic 3D arrays of iron nanorods", *Nano Lett.* 2002, *2(12),* 1393-1395
34. L.Vayssieres, "Growth of arrayed nanorods and nanowires of ZnO from aqueous solutions", *Adv. Mater.* 2003, *15(5)*, 464-466
35. L.Vayssieres, K. Keis, S.-E.Lindquist, A. Hagfeldt, "Purpose-Built Anisotropic Metal Oxide Material: 3D highly oriented Microrod-array of ZnO", *J. Phys. Chem. B* 2001, *105(17),* 3350-3352
36. L.Vayssieres, K. Keis, A. Hagfeldt, S.-E. Lindquist, "Three-dimensional Array of highly oriented crystalline ZnO Microtubes", *Chem. Mater.* 2001, *13(12),* 4395-4398
37. L.Vayssieres, "Aqueous Purpose-built Metal Oxide Thin Films", *Int. J. Mater. Prod. Technol.* 2003, *18(4-6)*, 313-337
38. L. Rabenberg, L.Vayssieres, "Multiple orientation relationships among nanocrystals of manganese oxides", *Microsc. Microanal*. 2003, *9(2)*, 402-403
39. L.Vayssieres, A. Manthiram, "2-D mesoparticulate arrays of α-Cr_2O_3", *J. Phys. Chem. B* 2003, *107(12)*, 2623-2625
40. L.Vayssieres, M. Graetzel, "Highly ordered SnO_2 nanorod-arrays from controlled aqueous growth", *Angew. Chem. Int. Ed.* 2004*, 43(28),* 3666-3670
41. L.Vayssieres, A. Hagfeldt, S.-E. Lindquist, "New Purpose-Built Nanostructured Metal Oxide materials for photoelectrochemical applications", *The Electrochemical Society Meeting Abstracts* 1998, *98(2),* 747; K. Keis, L.Vayssieres, H. Rensmo, S.-E. Lindquist, A. Hagfeldt, "Photoelectrochemical properties of nano-to-microstructured ZnO electrodes", *J. Electrochem. Soc*. 2001, *148(2),* A149-A155; K. Keis, L.Vayssieres, S.-E. Lindquist, A. Hagfeldt, "Nanostructured ZnO electrodes for photovoltaic applications", *Nanostruct. Mater.* 1999, *12(1-4),* 487-490
42. L.Vayssieres, "Advanced metal oxide based structures for sensor technologies", *Chemical Sensors* 2004*, 20(B),* 324-325
43. L.Vayssieres, "Advanced semiconductor nanostructures", *Comptes Rendus Chimie* 2006, 9(5-6), 691-701
44. C. L. Dong, C. Persson, L. Vayssieres, A. Augustsson, T, Schmitt, M. Mattesini, R. Ahuja, C. L. Chang, J.-H. Guo "The electronic structure of nanostructured ZnO from x-ray absorption and emission spectroscopy and the local density approximation", *Phys. Rev. B* 2004, *70(19)*, 195325
45. J.-H. Guo, L.Vayssieres, C. Persson, R. Ahuja, B. Johansson, J. Nordgren, "Polarization-dependent soft-x-ray absorption of highly oriented ZnO microrods" *J. Phys.: Condens. Matter* 2002, *14(28),* 6969-6974; C. Persson, C.L. Dong, L. Vayssieres, A. Augustsson, T, Schmitt, M. Mattesini, R. Ahuja, J. Nordgren, C.L. Chang, A. Ferreira da Silva, J.-H. Guo "x-ray absorption and emission spectroscopy of ZnO nanoparticles and highly oriented ZnO microrod arrays", *Microelectronics J.* 2006, *37(8)*, 686-689
46. L.Vayssieres, C. Saathe, S.M.Butorin, D.K.Shuh, J. Nordgren, J.-H.Guo "1D quantum confinement in αFe_2O_3 ultrafine nanorod array", *Adv. Mater*. 2005, *17(19)*, 2320-2323
47. L.Vayssieres, "On the thermodynamic stabilization of metal oxyhydroxides in solution", to be published
48. L.Vayssieres, "3-D Bio-Inorganic Arrays", in *Chemical Sensors VI: Chemical and Biological Sensors and Analytical Methods*, edited by C. Brukner-lea, P. Vanysek, G. Hunter, M. Egashira, N. Miura, and F. Mizutani (*The Electrochemical Society*, Pennington, NJ, 2004), pp. 322-343

49. T. Warwick, P. Heimann, D. Mossessian, W. McKinney, H. Padmore, "Performance of a high-resolution, high-flux density SGM undulator beamline at the ALS", *Rev. Sci. Instrum.* 1995, *66,* 2037-2040
50. J. Nordgren, G. Bray, S. Cramm, R. Nyholm, J. E. Rubensson, N. Wassdahl, "Soft x-ray emission spectroscopy using monochromated synchrotron radiation", *Rev. Sci. Instrum.* 1989, *60,* 1690-1696
51. L.Vayssieres, J.-H. Guo, J. Nordgren, "Purpose-built anisotropic metal oxide nanomaterials" in *Anisotropic Nanoparticles: Synthesis, Characterization and Applications*, edited by L. A. Lyon, S. J. Stranick, C. D. Keating and P. C. Searson, (*Mater. Res. Soc. Symp. Proc.* 635*,* Warrendale, PA, 2001), pp. 781-786
52. P. Kuiper, B. G. Searle, P. Rudolf, L. H. Tjeng, C. T. Chen, "X-ray magnetic dichroism of antiferromagnet Fe_2O_3: The orientation of magnetic moments observed by Fe 2*p* x-ray absorption spectroscopy", *Phys. Rev. Lett*. 1993, *70,* 1549-1552
53. L.-C. Duda, J. Nordgren, G. Drager, S. Bocharov, Th. Kirchner, "Polarized resonant inelastic X-ray scattering from single-crystal transition metal oxides", *J. Electron Spectrosc. Relat. Phenom.* 2000, *110-111*, 275-285.
54. J. P. Crocombette, M. Pollak, F. Jollet, N. Thromat, M. Gautier-Soyer, "X-ray-absorption spectroscopy at the Fe $L_{2,3}$ threshold in iron oxides", *Phys. Rev. B* 1995, *52,* 3143-3150.
55. J. E. Holliday, in *Band Structure Spectroscopy of Metals and Alloys,* (eds: D. J. Fabian, L. M. Watson), Academic Press, London 1973, p. 713.
56. H. W. Skinner, T. G. Bullen, J. Jonston, *Philos. Mag.* 1954, *45,* 1070.
57. E. Z. Kurmaev, V. R. Galakhov, A. Moewes, S. Shimada, K. Endo, S. S. Turner, P. Day, R. N. Lyubovskaya, D. L. Ederer, M. Iwami, "Electronic structure of molecular superconductors containing paramagnetic 3d ions", *Phys. Rev. B* 2000, *62,* 11380-11383
58. a) T. Åberg and B. Crasemann, in *Resonant Anomalous X-Ray Scattering*, (Eds: K. Fischer, G. Materlik, and C. Sparks), Elsevier, Amsterdam 1994, p. 431. b) A. Kotani, S. Shin, "Resonant inelastic x-ray scattering spectra for electrons in solids", *Rev. Mod. Phys.* 2001, *73*, 203-246. c) G. P. Zhang, T. A. Callcott, G. T. Woods, L. Lin, B. Sales, D. Mandrus, J. He, "Electron correlation effects in resonant inelastic x-ray scattering of NaV_2O_5", *Phys. Rev. Lett.* 2002, *88*, 077401. d) L.-C. Duda, T. Schmitt, J. Nordgren, G. Dhalenne, A. Revcolevschi, "Resonant inelastic soft X-ray scattering of insulating cuprates", *Surf. Rev. Lett.* 2002, *9*, 1103-1108. e) S. M. Butorin, "Resonant inelastic X-ray scattering as a probe of optical scale excitations in strongly electron-correlated systems: quasi-localized view", *J. Electron Spectrosc. Relat. Phenom.* 2000, *110–111*, 213-233. f) F. Gel'mukhanov, H. Ågren, "Resonant inelastic x-ray scattering with symmetry-selective excitation", *Phys. Rev. A* 1994, *49*, 4378-4389. g) W. A. Caliebe, C.-C. Kao, J. B. Hastings, M. Taguchi, A. Kotani, T. Uozumi, F. M. F. de Groot, "1*s*2*p* resonant inelastic x-ray scattering in α-Fe_2O_3, *Phys. Rev. B* 1998, 58, 13452-13458; h) K. Hamalainen, D. P. Siddons, J. B. Hastings, and L. E. Berman, Elimination of the inner-shell lifetime broadening in x-ray-absorption spectroscopy", *Phys. Rev. Lett.* 1991 67, 2850-2853. i) K. Hamalainen, C. C. Kao, J. B. Hastings, D. P. Siddons, L. E. Berman, V. Stojanoff, S. P. Cramer, "Spin-dependent x-ray absorption of MnO and MnF_2", *Phys. Rev. B* 1992, 46, 14274-14277.
59. a) S. M. Butorin, J.-H. Guo, M. Magnuson, P. Kuiper, J. Nordgren, "Low-energy d-d excitations in MnO studied by resonant x-ray fluorescence spectroscopy", *Phys. Rev. B* 1996, *54,* 4405-4408. b) P. Kuiper, J.-H. Guo, C. Saathe, L.-C. Duda, J. Nordgren, J. J. M. Pothuizen, F. M. F. de Groot, G. A. Sawatzky, "Resonant X-ray Raman spectra of Cu dd excitations in $Sr_2CUO_2Cl_2$", *Phys. Rev. Lett.* 1998, *80*, 5204-5207
60. L. A. Marusak, R. Messier, W. B. White, "Optical-absorption spectrum of hematite near IR to UV", *J. Phys. Chem. Solids* 1980, *41,* 981-984; A. A. Akl, "Optical properties of crystalline and non-crystalline iron oxide thin films deposited by spray pyrolysis", *Appl. Surf. Sci.* 2004, *233*, 307-319
61. T. Lindgren, H. Wang, N. Beermann, L.Vayssieres, A. Hagfeldt, S.-E. Lindquist, "Aqueous photoelectrochemistry of hematite nanorod-array", *Sol. Energy Mater. Sol. Cells* 2002, *71(2)*, 231-243; T. Lindgren, L.Vayssieres, H. Wang, S.-E. Lindquist, "Photo-oxidation of water at Hematite electrodes", in *Chemical Physics of Nanostructured Semiconductors,* edited by A. I. Kokorin and D. W. Bahnemann, (VSP-International Science Publishers, 2003), pp. 83-110